Understanding and controlling indium incorporation and surface segregation on $In_xGa_{1-x}N$ surfaces: An *ab initio* approach

Andrew Ian Duff,[*] Liverios Lymperakis, and Jörg Neugebauer
Max-Planck-Institut für Eisenforschung, Max-Planck-Str. 1, Düsseldorf 40237, Germany
(Received 10 October 2013; revised manuscript received 8 January 2014; published 13 February 2014)

The incorporation of In into the technologically relevant (0001) (Ga-polar) and $(000\bar{1})$ (N-polar) surfaces of $In_{0.25}Ga_{0.75}N$ is investigated using density functional theory. The cases of coherent pseudomorphic growth on GaN and on lattice-matched heterointerfaces are considered. For pseudomorphic growth on GaN, In incorporation into the {0001} surface layers is limited to a tiny growth window corresponding to extreme In-rich growth conditions and at the In-rich/Ga-poor region of the metal chemical potentials. Lattice-matched growth, however, allows for a wider growth window. Surface phase diagrams are constructed as a function of growth conditions and reveal similarities between the two polar growth planes. However, a strong driving force is found for segregation of In atoms to the first III-N layer for Ga-polar growth, but not for N-polar growth. The former was found to be mainly due to chemical effects (stronger Ga-N as compared to In-N bonds), absent in the case of N-polar growth. Furthermore, finite-temperature calculations show that In incorporated into the first III-N layer is stable to ≈ 150 K higher temperatures in the N-polar surface than in the Ga-polar surface, indicating that for a given level of In incorporation, higher temperatures can be used for N-polar growth as compared to Ga-polar growth.

DOI: 10.1103/PhysRevB.89.085307 PACS number(s): 68.35.bg, 68.35.Ja, 71.15.Mb, 68.47.Fg

I. INTRODUCTION

There is great interest in using InGaN as the active layer in optoelectronic devices: Owing to a tunable direct band gap ranging from 0.7 eV for InN [1–3] to 3.4 eV for GaN [4], almost the entire spectral range can be accessed by varying the In concentration [5,6]. Hence, these alloys have attracted considerable interest for use in light emitters, i.e., light-emitting diodes (LEDs) and laser diodes (LDs), specifically in the blue/green region of the optical spectrum as well as for high-efficiency solar cell applications [7–9].

However, the growth of high-quality $In_xGa_{1-x}N$ films with high-In content, as needed to access the green region of the spectrum, has proved challenging. The size difference between In and Ga as well as the difference in In-N and Ga-N bond strengths has been suggested to result in In surface segregation, limited In incorporation as well as spinodal decomposition and phase separation (see Ref. [10] and references therein). Furthermore, InN is the least thermally stable amongst the III-nitride semiconductors, with thermal decomposition of (0001) InN films starting at temperatures as low as 470 °C [11]. Hence, relatively low growth temperatures compared to GaN are required. The necessity of low growth temperatures substantially influences the adatom kinetics and results in rough surface morphologies and impaired crystal quality. In addition to the growth temperature, the growth of $In_xGa_{1-x}N$ surfaces depends strongly on the metal and nitrogen partial pressures. For example, it has been shown that the InN molar fraction increases with increasing ammonia [12] and nitrogen [13] fluxes in molecular beam epitaxy (MBE).

The technologically most relevant growth surface for III-nitrides is the (0001) (i.e., Ga-polar) surface [14]. However, recent experimental evidence suggests enhanced In incorporation through the crystallographically inequivalent $(000\bar{1})$ (N-polar) surface, for both metal-organic chemical vapor deposition (MOCVD) [15] and plasma-assisted MBE [16–18]. Furthermore, N-polar InN growth allows temperatures ≈ 100 °C higher than the thermal dissociation limit of In-polar InN surfaces [17–21].

Thus, the growth of high-quality, In-rich $In_xGa_{1-x}N$ films constitutes a puzzling situation where the complex interplay between surface morphologies, partial pressures, and growth temperatures plays a central role. A first step in achieving full control on the growth and properties of polar $In_xGa_{1-x}N$ surfaces is to gather a fundamental understanding of the relevant atomistic surface processes that govern the surface morphologies and the In incorporation and segregation processes, as well as to identify and investigate the pronounced differences in the growth of the two polar faces.

The majority of first-principles studies have focused solely on the surface reconstructions and the electronic structure of {0001} GaN and/or InN surfaces [22–35]. A few studies have also considered the role of In as a surfactant for GaN growth [36–38]. These studies indicated that the presence of a metal adlayer on the Ga-polar surface provides a faster subsurface diffusion channel for N atoms than would otherwise be available on the surface, resulting in smoother surface morphologies and higher crystal quality. Gan and Srolovitz provided a comparative study of cation adsorption on Ga- and N-polar GaN and InN surfaces [39]. However, the issues of In incorporation and segregation, the effect of in-plane strain, as well as the formation of more than one metal adlayer (factors which may substantially alter the growth phase diagrams) were not considered.

A few studies explicitly addressing In incorporation at Ga-polar (0001), nonpolar $(10\bar{1}0)$, as well as semipolar $(10\bar{1}1)$ and $(1\bar{2}22)$ GaN and $In_xGa_{1-x}N$ surfaces have been reported [40–42]. These studies revealed that under extremely In-rich and Ga-poor conditions, surface structures consisted of an In bilayer and In adlayer for the Ga-polar *c*-plane and *m*-plane surfaces, respectively (consistent with experimental findings of In adlayers/bilayers stable on InGaN surfaces[13,38,43–46]),

[*]Current address: Department of Materials, Imperial College London, UK; andrew.duff@imperial.ac.uk

 ©2014 American Physical Society

both with In substituting for Ga in the first surface layer (In_{Ga}) [40,41]. Furthermore, it has been shown that In incorporation at semipolar surfaces and/or c-plane step edges is energetically more favorable than at polar and nonpolar GaN surfaces [40,42]. However, these studies, focusing on the Ga-polar surfaces, considered only a limited set of surface morphologies built from a single species of cation, including adatoms, adlayers, bilayers, and a single In_{Ga} in the first surface layer. The effects of In_{Ga} residing in deeper layers, as well as the effect of strain on the surface energetics, were not considered.

In this work, an extensive first-principles study investigating surface energetics, In incorporation, and surface segregation for the Ga-polar and N-polar surfaces of $In_{0.25}Ga_{0.75}N$ has been undertaken. A concentration of 25% In was chosen because it corresponds to blue-green emission (at approximately 500 nm) and furthermore it enables better modeling of the energetics of already incorporated In [47]. A large range of surface morphologies and reconstructions have been considered, including In and Ga adlayers, bilayers, trilayers, adatoms, and vacancies. In addition, cation adlayer/s consisting of mixtures of Ga and In are considered, and the effect of already incorporated In is fully included by also considering reconstructions containing In in subsurface layers. The effect of in-plane strain is also investigated by fixing the in-plane lattice parameters either to those of GaN or to those of $In_{0.25}Ga_{0.75}N$. The former corresponds to pseudomorphic growth of $In_{0.25}Ga_{0.75}N$ on GaN, whereas the latter corresponds to growth of $In_{0.25}Ga_{0.75}N$ on lattice-matched heterointerfaces (such as, approximately, the lattice-matched growth of $In_{0.25}Ga_{0.75}N$ on ZnO [48,49]).

The structure of the paper is as follows: In Sec. II, the details of the calculations along with the formalism of the surface thermodynamics will be provided. In Sec. III, the thermodynamically allowed regions of $In_{0.25}Ga_{0.75}N$ growth will be carefully defined, and the surface phase diagrams will be presented. In Sec. IV, the results will be extended to finite temperature by inclusion of entropic effects. A detailed discussion on the energetics of indium surface segregation will then be given in Sec. V. Finally, concluding remarks will be presented in Sec. VI.

II. CALCULATIONS

Density functional theory (DFT) is used within the local density approximation (LDA) [50,51] and the projector augmented-wave (PAW) method [52,53], with Ga and In d electrons included as valence states. The surfaces are modeled using a slab geometry consisting of eight III-N bilayers and a vacuum region of 20 Å. A plane-wave energy cutoff of 450 eV was used and k points were sampled using an equivalent $4 \times 4 \times 1$ Monkhorst-Pack mesh [54] for the 2×2 surface unit cell. For Ga-polar (N-polar) surfaces, the lowermost N (Ga) atoms were passivated with pseudohydrogen atoms of partial charge 0.75 (1.25). Convergence with respect to k-point sampling, energy cutoff, vacuum, and slab thickness were explicitly tested and found to provide surface energies with an accuracy better than 3 meV/Å^2.

To construct the slabs and investigate both $In_{0.25}Ga_{0.75}N$ growth pseudomorphic to GaN and $In_{0.25}Ga_{0.75}N$ grown on lattice-mismatched heterointerfaces, the equilibrium lattice constants of both bulk GaN and $In_{0.25}Ga_{0.75}N$ were first

TABLE I. Lattice parameters and formation enthalpies at zero temperature calculated for GaN, InN, and $In_{0.25}Ga_{0.75}N$ for three different strain configurations. The formation enthalpies of $In_xGa_{1-x}N$ are calculated as $\Delta H_f = E_{\rm tot}^{{\rm In}_x{\rm Ga}_{1-x}{\rm N}} - xE_{\rm tot}^{\rm In\text{-}bulk} - (1-x)E_{\rm tot}^{\rm Ga\text{-}bulk} - \frac{1}{2}E_{\rm tot}^{\rm N_2mol}$, where $E_{\rm tot}^{\rm In\text{-}bulk}$ and $E_{\rm tot}^{\rm Ga\text{-}bulk}$ are the total energies of bct In and α-Ga at their equilibrium lattice constants and $E_{\rm tot}^{{\rm In}_x{\rm Ga}_{1-x}{\rm N}}$ is the total energy of the SQS wurtzite $In_xGa_{1-x}N$ alloy. For the latter, and also for GaN and InN, calculations are performed either biaxially strained to GaN (denoted as @ $a_{\rm GaN}^{\rm lat}$), to $In_{0.25}Ga_{0.75}N$ (denoted as @ $a_{{\rm In}_{0.25}{\rm Ga}_{0.75}{\rm N}}^{\rm lat}$), or with the equilibrium in-plane lattice constant (denoted as @ $a_{\rm eq}^{\rm lat}$). For the $In_{0.25}Ga_{0.75}N$ SQS structures, a unique u lattice parameter can not be defined and is not shown.

	a (Å)	c (Å)	u	ΔH_f (eV)
GaN @ $a_{\rm eq}^{\rm lat}$	3.1565	5.1400	0.3765	−1.703
GaN @ $a_{{\rm In}_{0.25}{\rm Ga}_{0.75}{\rm N}}^{\rm lat}$	3.2456	5.0754	0.3834	−1.654
InN @ $a_{\rm eq}^{\rm lat}$	3.5130	5.6654	0.3788	−0.445
InN @ $a_{\rm GaN}^{\rm lat}$	3.1565	6.1131	0.3394	0.136
InN @ $a_{{\rm In}_{0.25}{\rm Ga}_{0.75}{\rm N}}^{\rm lat}$	3.2456	6.0077	0.3485	−0.133
$In_{0.25}Ga_{0.75}N$ @ $a_{\rm eq}^{\rm lat}$	3.2456	5.2608		−1.322
$In_{0.25}Ga_{0.75}N$ @ $a_{\rm GaN}^{\rm lat}$	3.1565	5.3497		−1.278

calculated. The corresponding lattice constants for GaN, InN, and $In_{0.25}Ga_{0.75}N$ are shown in Table I. In order to model a bulk random $In_{0.25}Ga_{0.75}N$ alloy, the 16 dimer special quasirandom structure (SQS) reported by Gan *et al.* [55] is utilized. The calculated lattice constants are in agreement with previous LDA calculations [55] and underestimate by $\approx 1\%$ the corresponding experimental values (see Ref. [56] and references therein). Furthermore, negligible bowing of the lattice constants is found in all cases, including both the a and c equilibrium lattice constants and also the c lattice constants of the biaxially strained configurations.

To model different surface geometries with varying degrees and configurations of incorporated In_{Ga}, slabs consisting of eight III-N bilayers were constructed. A large number of surface morphologies and reconstructions were calculated, using in-plane periodicities of either 1×1 for adlayers, bilayers, and trilayers, 2×2 for adatoms and mixed Ga/In adlayer/s, or $\sqrt{3} \times \sqrt{3}$ for laterally contracted bilayers (LCBs) [28]. In addition, both 2×2 and $\sqrt{3} \times \sqrt{3}$ periodicities were also used for the case of structures with incorporated In_{Ga}. For calculations of $In_{0.25}Ga_{0.75}N$ grown pseudomorphically on GaN, the lattice parameters of bulk GaN were used to construct the initial slab geometry, whereas for the lattice-matched case, the supercell was constructed using the in-plane lattice parameters of $In_{0.25}Ga_{0.75}N$. For each surface geometry, the most favorable configuration of incorporated In_{Ga} was sought by calculating not just the stability of 25% In incorporation across the eight III-N bilayers, but also competing concentrations and configurations of In_{Ga} within the topmost layers. For both the pseudomorphic and lattice-matched cases, all atoms except for the pseudohydrogen atoms were allowed to fully relax during the calculation, although with in-plane lattice parameters held fixed.

Owing to the low symmetry of the wurtzite structure, slabs and/or finite crystals bounded by only one type of polar facets [i.e., (0001) or $(000\bar{1})$] can not be constructed and

unique and physically meaningful absolute surface energies can not be defined for the (In)GaN-polar surfaces. Instead, surface energies must be calculated with respect to a reference structure, which can be arbitrarily chosen, since only the relative stability of different surface morphologies (for a given polarity and choice of in-plane lattice parameter) are relevant. Furthermore, the investigated surfaces are not necessarily stoichiometric. Hence, their surface energies depend on the corresponding chemical potentials μ_X (X = Ga, In, and N). These chemical potentials are related to the partial pressures of the carrier gases, allowing a mapping of stable surface morphologies and reconstructions to different growth regimes (In-rich, Ga-rich, N-rich, etc). The relative surface energy is expressed as

$$\Delta\gamma(\mu_{\rm Ga},\mu_{\rm N},\mu_{\rm In}) = E^{\rm tot}_{\rm surf} - E^{\rm tot}_{\rm ref} - \Delta n_{\rm Ga}\mu_{\rm Ga} - \Delta n_{\rm N}\mu_{\rm N} - \Delta n_{\rm In}\mu_{\rm In}, \quad (1)$$

where $E^{\rm tot}_{\rm surf}$ and $E^{\rm tot}_{\rm ref}$ are the total supercell energies of the surface reconstruction and the reference surface structure, respectively, and Δn_X and μ_X are the excess number of atoms of species X compared to the reference structure and the chemical potential of X, respectively.

The upper limits on the chemical potentials of Ga, In, and N correspond to Ga-, In-, and N-rich conditions and are the total energies per atom of bulk Ga, bulk In, and a nitrogen molecule, respectively, as calculated within DFT:

$$\Delta\mu_{\rm Ga} = \mu_{\rm Ga} - \mu^{\rm bulk}_{\rm Ga} \leqslant 0, \quad (2)$$

$$\Delta\mu_{\rm In} = \mu_{\rm In} - \mu^{\rm bulk}_{\rm In} \leqslant 0, \quad (3)$$

$$\Delta\mu_{\rm N} = \mu_{\rm N} - \mu^{\rm N_2 mol}_{\rm N} \leqslant 0. \quad (4)$$

In addition, we assume thermodynamic equilibrium with $In_{0.25}Ga_{0.75}N$ so that the following constraint to the chemical potentials is imposed:

$$\mu_{\rm In_{0.25}Ga_{0.75}N} = \tfrac{1}{4}\mu_{\rm In} + \tfrac{3}{4}\mu_{\rm Ga} + \mu_{\rm N}, \quad (5)$$

where $\mu_{\rm In_{0.25}Ga_{0.75}N}$ is the total energy per metal atom-N dimer of $In_{0.25}Ga_{0.75}N$. In this work, we treat $\mu_{\rm Ga}$ and $\mu_{\rm In}$ as independent variables, with $\mu_{\rm N}$ then uniquely determined by Eq. (5). N-rich conditions ($\mu_{\rm N} = \mu^{\rm N_2 mol}_{\rm N}$) therefore define the lower limits on the metal chemical potentials, with the $\mu_{\rm Ga}$ lower limit becoming a function of $\mu_{\rm In}$ (and vice versa):

$$\tfrac{3}{4}\Delta\mu_{\rm Ga} \geqslant \Delta H^f_{\rm In_{0.25}Ga_{0.75}N} - \tfrac{1}{4}\Delta\mu_{\rm In}, \quad (6)$$

where $\Delta H^f_{\rm In_{0.25}Ga_{0.75}N} = \mu_{\rm In_{0.25}Ga_{0.75}N} - \frac{1}{4}\mu^{\rm bulk}_{\rm In} - \frac{3}{4}\mu^{\rm bulk}_{\rm Ga} - \mu^{\rm N_2 mol}_{\rm N}$ is the formation enthalpy of $In_{0.25}Ga_{0.75}N$. Additional constraints applied to the chemical potentials arise from the requirement that the competing phases of InN and GaN are thermodynamically unstable:

$$\mu_{\rm Ga} + \mu_{\rm N} \leqslant \mu_{\rm GaN}, \quad (7)$$

$$\mu_{\rm In} + \mu_{\rm N} \leqslant \mu_{\rm InN}, \quad (8)$$

further substantially limiting the thermodynamic region pertaining to $In_{0.25}Ga_{0.75}N$ growth.

Previous LDA-DFT calculations have shown that, at 25% In concentration, one is within the miscibility gap of $In_xGa_{1-x}N$ alloys at typical growth temperatures [55]. However, previous theoretical and experimental work has provided strong evidence that phase separation can be suppressed during the pseudomorphic (i.e., biaxially strained) growth of cubic InGaN epitaxial layers on GaN [57]. Our own calculations support this, with the mixing enthalpy of wurtzite $In_xGa_{1-x}N$, pseudomorphic to GaN, calculated to be negative with a single minimum across the entire range of compositions x. This assumes, however, that the phase separation to GaN and InN is not accompanied by plastic relaxation of the biaxial strain. According to the work of Fischer *et al.* [58], the critical thickness for the onset of plastic relaxation of $In_{0.25}Ga_{0.75}N$ on GaN is estimated to be less than ≈ 6 nm. Hence, spinodal decomposition in bulk $In_{0.25}Ga_{0.75}N$ alloys is fully suppressed for growth on GaN of epilayers of maximum thickness of ≈ 6 nm.

For the chemical potentials of the In and Ga bulk phases, we use the calculated total energies of bct In and α-Ga at their calculated equilibrium lattice constants. The melting temperatures of In and Ga are ≈ 429 and ≈ 302 K [59], respectively, and at the typical growth temperatures of $In_{0.25}Ga_{0.75}N$ they are both in the liquid phase. The calculated chemical potentials of bulk Ga, In, and N_2 molecules are $\mu_{\rm Ga\text{-}bulk} = -3.359$ eV, $\mu_{\rm In\text{-}bulk} = -3.033$ eV, and $\frac{1}{2}\mu_{\rm N_2\text{-}mol} = -5.857$ eV, respectively. The cohesive and formation energies were corrected by spin-polarization energies of 2.89, 0.117, and 0.134 eV for the N, In, and Ga atoms, respectively [56]. Additionally, configurational entropic contributions within the regular solution model at $T = 1000$ K are applied to the chemical potentials of $In_{0.25}Ga_{0.75}N$ as well as to the surface energies.

III. SURFACE PHASE DIAGRAMS

Within the aforementioned scheme, surface phase diagrams have been constructed for both surface polarities showing the most stable surface reconstruction as a function of the two metal chemical potentials. The fields of stability of the various competing phases, as defined by Eqs. (2)–(4) and (7) and (8) are shown in Figs. 1(a) and 1(b) for the cases of $In_{0.25}Ga_{0.75}N$ pseudomorphic to GaN and lattice matched, respectively. Equations (2) and (3) are represented by gray regions, with Eq. (4) represented by blue regions. Within these regions, all surfaces are unstable with respect to Ga droplets, In droplets, and N_2 molecules, respectively. Furthermore, lines parallel to the N-rich line (labeled as "$\mu_{\rm N} = \mu^{\rm N_2 mol}_{\rm N}$" in the figures) are lines of constant $\mu_{\rm N}$, whereas lines drawn from the N-rich line to the upper-right corner (i.e., Ga- and In-rich limits) represent paths across which $\mu_{\rm In}/\mu_{\rm Ga}$ is held fixed but $\mu_{\rm N} - \mu^{\rm N_2 mol}_{\rm N}$ varies from zero (N-rich limit) to $\Delta H^f_{\rm In_{0.25}Ga_{0.75}N}$ (metal-rich limit).

For pseudomorphic growth on GaN, the formation enthalpy of InN is positive and it is intrinsically unstable against the competing phases of bulk In and molecular N_2. Thus, the boundary line defined by Eq. (8) lies within the bulk In and molecular N_2 regimes of the phase diagram [see Fig. 1(a)]. The boundary lines defined by Eqs. (2)–(5) and (7) enclose a triangle located at the extreme N-rich region and at the

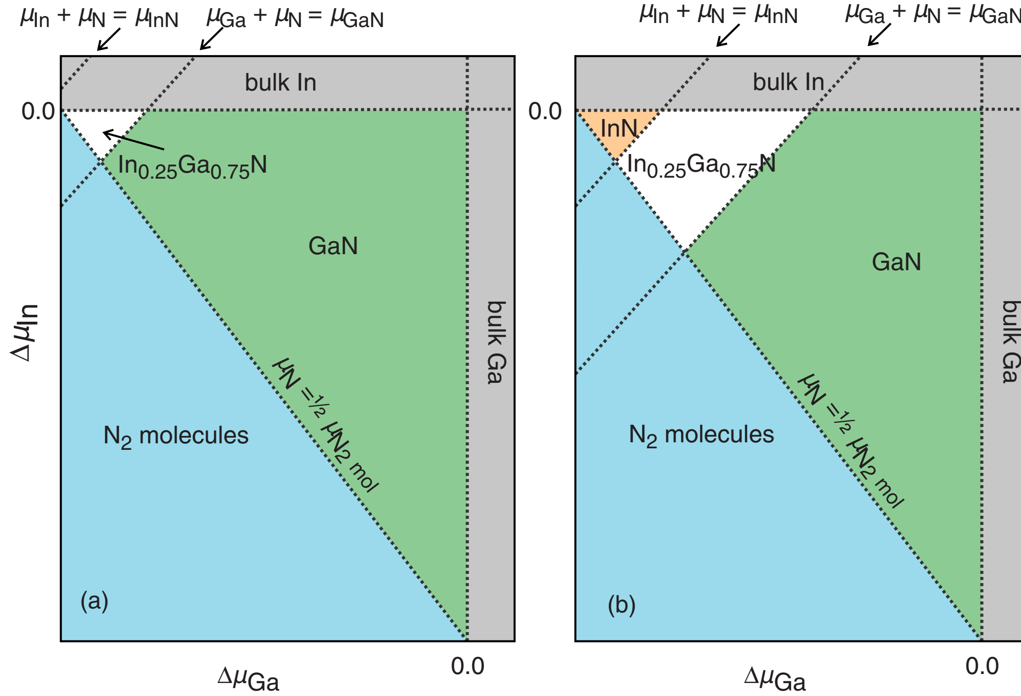

FIG. 1. (Color online) Schematic representation of the different regimes in the phase diagrams of $In_{0.25}Ga_{0.75}N$ alloys (a) pseudomorphically grown on GaN and (b) strain free (i.e., lattice matched). Dotted lines indicate the onset of thermodynamic stability for each of the various phases, with differently shaded areas indicating the fields of thermodynamic stability for each phase.

In-rich/Ga-poor region of the metal chemical potentials and represents the window of chemical potentials within which $In_{0.25}Ga_{0.75}N$ biaxially strained to GaN is thermodynamically stable. The width of the In and Ga chemical potentials within the aforementioned window is $\Delta\mu \approx 0.15$ eV, which is one order of magnitude smaller than the range of Ga chemical potentials for growth of GaN ($\Delta\mu_{Ga} \approx 1.5$ eV).

For lattice-matched growth [(see Fig. 1(b)], the formation enthalpy of InN is negative, so that, in this case, the growth window of $In_{0.25}Ga_{0.75}N$ is a trapezoid enclosed by the boundary lines defined by Eqs. (2)–(5), (7), and (8). In contrast to the former case, the growth of lattice-matched $In_{0.25}Ga_{0.75}N$ is shifted towards more moderate In-rich/Ga-poor conditions. Furthermore, the corresponding growth window is wider (the range of In and Ga chemical potentials is $\Delta\mu \approx 0.5$ eV).

In the following, results will be presented first for pseudomorphic growth on GaN (the strained case) and subsequently for the lattice-matched case.

A. Pseudomorphic $In_{0.25}Ga_{0.75}N$ on GaN

The surface phase diagrams for the growth of Ga-polar (0001) and N-polar (000$\bar{1}$) $In_{0.25}Ga_{0.75}N$ are shown in Figs. 2(a)–2(d). Figures 2(a) and 2(b) cover a large range of μ_{Ga} and μ_{In} values, including a large portion of the GaN stable region, whereas Figs. 2(c) and 2(d) focus on a zoomed-in region of the phase diagram centered on the $In_{0.25}Ga_{0.75}N$ stable region.

Considering first Figs. 2(a) and 2(b), one sees that for In-poor conditions, i.e., for small values of μ_{In}, qualitative agreement with previous calculations of pure GaN surfaces is obtained [22,30,60,61] (although in these previous calculations thermodynamic equilibrium with respect to GaN rather than $In_{0.25}Ga_{0.75}N$ was considered). For the Ga-polar surface [Fig. 2(a)], a laterally contracted Ga bilayer (LCB) is found to be stable under Ga-rich conditions, with a 2×2 Ga adatom stable under Ga-moderate conditions and a 2×2 N adatom stable under Ga-moderate to Ga-poor conditions. For the N-polar surface [Fig. 2(b)], a Ga adlayer is found to be stable under Ga-rich and Ga-moderate conditions, with a 2×2 Ga adatom stabilized under N-rich conditions.

For the Ga-polar surface, one sees that, under Ga-rich conditions, the Ga LCB region is stable across the entire range of allowed μ_{In} values. For In-rich conditions, excess In is also stabilized in the form of a relaxed LCB layer, although relaxation of the LCB in this case in fact results in formation of an In bilayer with an In adatom on top (for simplicity, however, we retain the "In LCB" nomenclature). For In-rich and Ga-moderate/-rich conditions, a crossover region exists, in which a mixed In/Ga LCB structure becomes preferentially stabilized, consisting of an In LCB (A2-A3) on top of a Ga adlayer (A1), as shown in Fig. 3(c).

The stability of a Ga LCB under Ga-rich conditions has already been connected to the self-surfactant effect of Ga during GaN growth [28] and explains the observed smooth surface morphologies and high crystal quality for growth within this region. In addition, the region for which the In LCB is found to be stable provides the growth window for which In acts as a surfactant during GaN growth. Specifically, In-rich and Ga-moderate to Ga-rich conditions (to avoid the onset of In incorporation under Ga-poor conditions) are required.

For the N-polar surface, and under Ga-rich conditions, the Ga adlayer is stable between In-poor and In-moderate

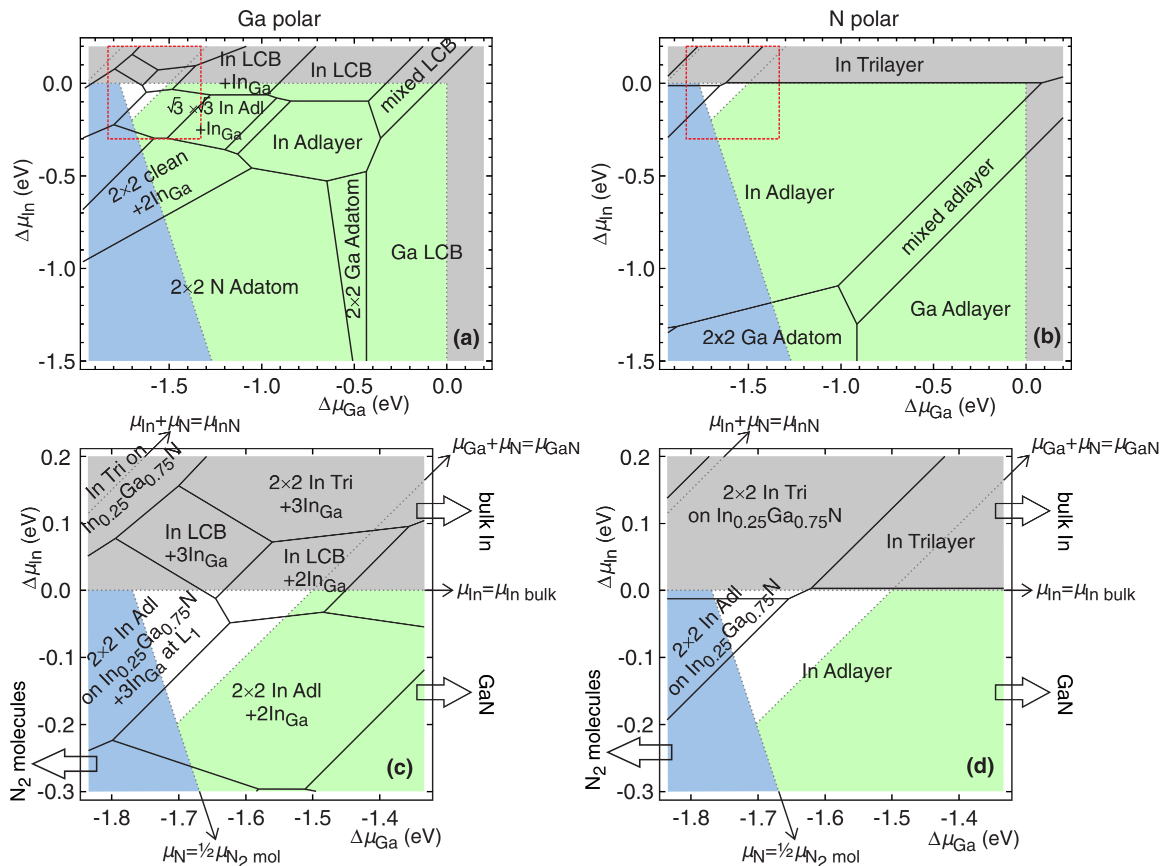

FIG. 2. (Color online) Surface phase diagrams for Ga-polar [(a) and (c)] and N-polar [(b) and (d)] $In_{0.25}Ga_{0.75}N$ pseudomorphically grown on GaN. Figures (a) and (b) correspond to a range of μ_{In} and μ_{Ga} values including both the region corresponding to $In_{0.25}Ga_{0.75}N$ growth (small white triangular region), and also the regions for which $In_{0.25}Ga_{0.75}N$ is unstable against GaN (green shaded area). In addition, blue (gray) shaded areas are used to denote instability with respect to N_2 molecules (bulk In and Ga). Figures (c) and (d) instead show zoomed-in views of the regions denoted by the dashed red rectangles in (a) and (b).

conditions, whereupon a mixed Ga/In adlayer becomes stable. This structure consists of a 2×2 metal adlayer with one of the A1 sites occupied by In and the other three by Ga [see Fig. 3(f)]. Under In- and Ga-rich conditions, an In adlayer becomes stable, and remains stable under In-rich conditions for almost the entire range of μ_{Ga} values. The In trilayer becomes the lowest-energy structure only for $\mu_{In} > \mu_{In}^{bulk}$, and is therefore unstable with respect to In droplet formation. Interestingly, the transition from In adlayer to In trilayer is abrupt, with the In bilayer found to be unstable for all values of the chemical potentials. This can be attributed to the much stronger binding of the first In adlayer (binding energy 4.85 eV per atom) on the bare N-polar surface in comparison to the binding of the second In adlayer on the first In adlayer (binding energy 2.91 eV per atom). Hence, the stability of the In adlayer is extended towards more In-rich conditions and completely removes the region where an In bilayer is stable. For the Ga-polar surface, incorporated In_{Ga} becomes stable as one approaches more Ga-poor conditions. From Figs. 2(a) and 2(c), one sees that under Ga-poor/-moderate conditions, In_{Ga} in L_1 is stabilized across a band of surface morphologies (see Fig. 3 for layer labeling convention). These include the 2×2 clean + 2 In_{Ga}, 2×2 In adlayer + 2 In_{Ga}, and In LCB + 2 In_{Ga} structures. For N-polar surfaces, however, no In_{Ga} atoms are found to be stable under Ga-poor/-moderate conditions [Fig. 2(b)].

Within the $In_{0.25}Ga_{0.75}N$ stable region for Ga polar [see Fig. 2(c)], one finds that fully incorporated $In_{0.25}Ga_{0.75}N$ with 3 In_{Ga} at L_1 underneath an In adlayer becomes stable [see Fig. 3(b)]. Similar, for N polar [see Fig. 2(d)] fully incorporated $In_{0.25}Ga_{0.75}N$ beneath an In adlayer is energetically favorable within the $In_{0.25}Ga_{0.75}N$ stable region [see Fig. 3(e)], but In concentrations greater than 25% are not found favorable within any layer of the slab. These results indicate that (i) growth of $In_{0.25}Ga_{0.75}N$ is energetically favorable for extreme In- and N-rich and Ga-poor conditions and (ii) Ga-polar surfaces can incorporate more In within the first III-N layer (i.e., layer L_1).

In order to provide a deeper understanding of the aforementioned apparent result regarding the higher In content in the first layer for Ga-polar surfaces, we analyze the total energies of GaN slabs with up to four In_{Ga} and with various distributions within the topmost four III-N layers (i.e., layers L_1–L_4). Our calculated total energies indicate enhanced stability of In_{Ga} in L_1 for the Ga-polar surface. For example, the 2×2 In adlayer with four In_{Ga} atoms in L_1 is by 0.21 eV per 1×1 lower in energy than the 2×2 In adlayer with four In_{Ga} atoms evenly distributed in the topmost four III-N layers (layers L_1–L_4). This is particularly surprising because multiple In_{Ga} atoms in

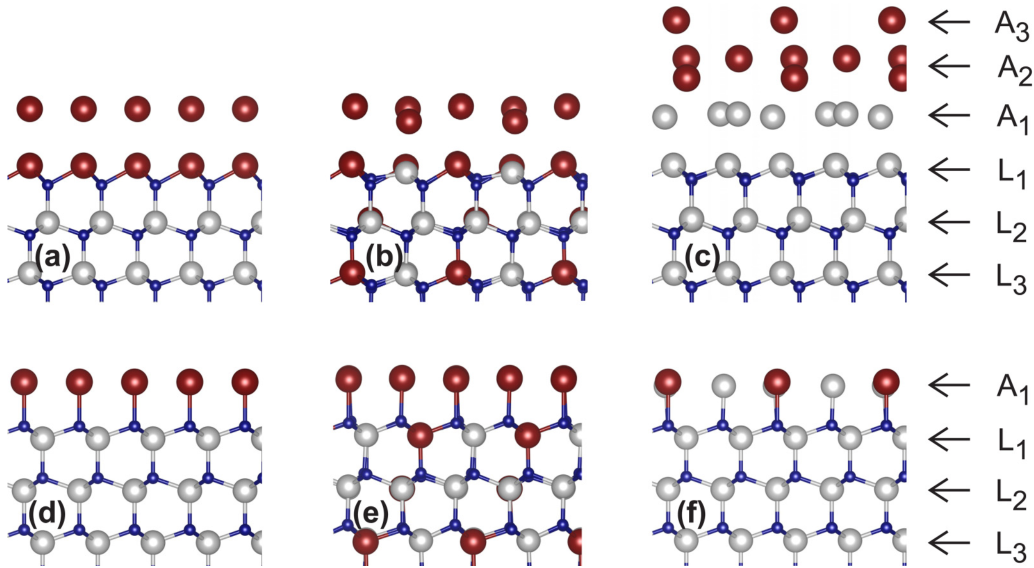

FIG. 3. (Color online) Ball-and-stick models for selected Ga-polar [(a)–(c)] and N-polar [(d)–(f)] morphologies for the case of coherent pseudomorphic growth on GaN. Morphologies correspond to (a) 1×1 In adlayer + In_{Ga}; (b) 2×2 In adlayer on $In_{0.25}Ga_{0.75}N$ + 3 In_{Ga} in L_1; (c) mixed In/Ga LCB (consisting of a contracted In adlayer on top of a Ga adlayer); (d) In adlayer; (e) In adlayer on $In_{0.25}Ga_{0.75}N$; and (f) mixed In/Ga adlayer. Small dark, large dark, and large light balls correspond to N, In, and Ga atoms, respectively. L_1, L_2, and L_3 denote the first, second, and third III-N layers, i.e., layers where the metal atoms form three or four bonds with N atoms. A1, A2, and A3 denote the first, second, and the third metallic adlayers.

L_1 will experience an In_{Ga}-In_{Ga} repulsion due to the In/Ga size mismatch. Therefore, the energy gain due to first layer occupancy of In_{Ga}, arising either from strain relaxation or from a more favorable bonding configuration (with the balance between these effects to be discussed in more detail in Sec. V), must compensate for this In_{Ga}-In_{Ga} repulsion. In contrast, for N-polar surfaces, no such enhanced stability in the first layer is found and the In_{Ga} atoms are evenly distributed within the slab.

B. Lattice-matched $In_{0.25}Ga_{0.75}N$

For $In_{0.25}Ga_{0.75}N$ with in-plane lattice parameters consistent with 25% In concentration (i.e., $In_{0.25}Ga_{0.75}N$ grown on a lattice-matched heterointerface), qualitatively the same picture emerges [see Figs. 4(a)–4(d)]. However, we should note that for this lattice-matched case, the presence of the InN growth region now advances into the In-rich, Ga-poor side of the $In_{0.25}Ga_{0.75}N$ growth region, meaning that tuning of growth parameters too far in this direction will now result in spinodal decomposition rather than In droplet formation.

Fully incorporated $In_{0.25}Ga_{0.75}N$ (with an In adlayer) is again stabilized for N-polar surfaces within the allowed region for $In_{0.25}Ga_{0.75}N$ growth, but here over a wider range of chemical potentials than for the case of pseudomorphic growth on GaN. Specifically, at the In- and N-rich limits of the allowed region for $In_{0.25}Ga_{0.75}N$ growth one finds fully incorporated $In_{0.25}Ga_{0.75}N$ with three In_{Ga} at L_1 and two In_{Ga} at L_2 and L_3. For less In-rich conditions, the incorporation of In_{Ga} exceeding a concentration of 25% in any layer of the slab is energetically unfavorable.

For Ga-polar surfaces, structures with In composition in the first two III-N layers (layers L_1 and L_2) exceeding 25% are now found to be stable within the $In_{0.25}Ga_{0.75}N$ growth region. Specifically, two surface structures are energetically the most stable within the $In_{0.25}Ga_{0.75}N$ growth window: (i) the $In_{0.25}Ga_{0.75}N$ underneath an In adlayer with 100% In composition in L_1 and 75% in L_2 and (ii) fully incorporated $In_{0.25}Ga_{0.75}N$ underneath an In adlayer with 75% In composition in L_1. The increased In incorporation in the topmost III-N layers for both polarities as compared to the case of coherent growth on GaN can be explained in terms of the compressive strain induced by the much larger In atoms, which can be more efficiently accommodated by the larger basal-plane lattice constant of $In_{0.25}Ga_{0.75}N$ as compared to GaN.

IV. TEMPERATURE EFFECTS

The phase diagrams derived in Sec. III provide valuable information regarding the surface morphologies and reconstructions for various growth conditions in terms of the chemical potentials. However, in order to investigate the thermal stability of incorporated In, temperature and partial pressures have to be explicitly included in our model. Our phase diagrams indicate that full incorporation of $In_{0.25}Ga_{0.75}N$ takes place underneath an In adlayer. Thus, in order to model the thermodynamics at the onset of In incorporation, we determine the thermal stability of a single In_{Ga} atom incorporated in L_1 at both (0001) and $(000\bar{1})$ surfaces underneath an In adlayer with a 2×2 surface periodicity. In this section, calculations are performed for the case of $In_{0.25}Ga_{0.75}N$ grown pseudomorphic to GaN.

MBE is regarded as a nonequilibrium growth technique operating under a large thermodynamic driving force, i.e., the Gibbs free-energy difference between the gaseous species and the solid phase product is large compared to other growth

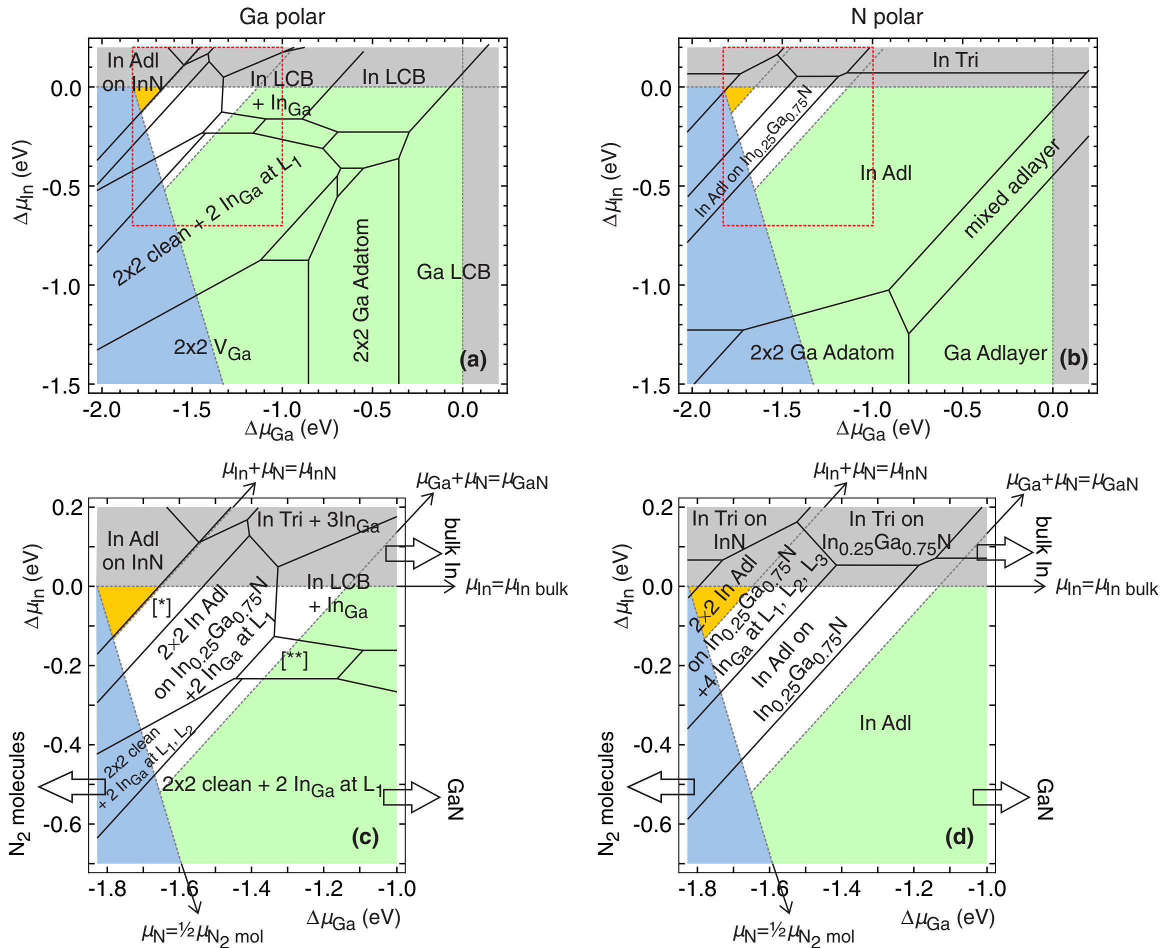

FIG. 4. (Color online) Surface phase diagrams for Ga-polar [(a), (c)] and N-polar [(b), (d)] $In_{0.25}Ga_{0.75}N$ for the lattice-matched case (biaxially strained to $In_{0.25}Ga_{0.75}N$). Figures (c) and (d) show a zoomed-in view of the region denoted by the dashed red rectangle in (a) and (b). The white trapezoid denotes the region of chemical potentials for which $In_{0.25}Ga_{0.75}N$ is stable, while the green, orange, and blue shaded regions indicate that $In_{0.25}Ga_{0.75}N$ is unstable against the formation of GaN, InN, and N_2 molecules, respectively. In the gray shaded regions, $In_{0.25}Ga_{0.75}N$ is unstable with respect to bulk Ga and bulk In. In (c), [*] denotes the 2×2 In adlayer on $In_{0.25}Ga_{0.75}N$ with 4 In_{Ga} in L_1 and 3 In_{Ga} in L_2 and [**] denotes the 2×2 In adlayer with 2 In_{Ga} in L_1.

techniques such as liquid phase epitaxy and hydride vapor phase epitaxy [62]. However, as shown in Ref. [63], useful guidance can be obtained by applying the thermodynamic framework to MBE. In the following, the partial pressures $\tilde{p}$ refer to the actual values at the growth front, i.e., the solid/gas interface, where near-equilibrium conditions are assumed [64]. It has to be noted here that $\tilde{p}$ does not necessarily correspond to the experimentally measured beam equivalent partial pressure. In order to map the chemical potentials of the gaseous species into partial pressures $\tilde{p}$ and temperatures T, we use the ideal gas approximation, which is valid for MBE due to the low pressures and relatively high temperatures used.

In order to calculate the effect of the vibrational contributions to the surface energy, we have calculated the dynamical matrix for all surfaces under consideration. In order to calculate the force constant matrix of a surface, one in principle needs to consider a semi-infinite supercell. However, contributions arising from deeper layers are expected to be the same for all surface structures, and to correspond to those of a bulk system. Thus, ΔF^{vib} is expected to converge with respect to the number of surface layers considered in the force matrix calculation. Furthermore, as has been pointed out in Sec. II, unique and physically meaningful absolute surface energies can not be defined for the (In)GaN polar surfaces. However, free-energy differences are physically meaningful. Thus, in the following we derive the difference in surface free energies $\Delta F = F_{2\times2\ \text{In adl+In}_\text{Ga}} - F_{\text{clean}}$ between a 2×2 In adlayer with an In_{Ga} atom in L_1 and a clean surface for both (0001) and $(000\bar{1})$ surfaces:

$$\Delta F = \Delta E^{\text{tot}} + \Delta F^{\text{vib}} - \sum_i \Delta n_i \mu_i, \quad (9)$$

where $\Delta F^{\text{vib}} = F^{\text{vib}}_{2\times2\ \text{In adl+In}_\text{Ga}} - F^{\text{vib}}_{\text{clean}}$ is the difference in the vibrational contributions to the free energy between the 2×2 In adlayer with In_{Ga} and the clean surface morphologies. The vibrational contributions to the free energies have been calculated within the harmonic approximation [65] where the force constant matrix and in turn the dynamical matrix have been calculated with the small displacement method (see Ref. [66] and references therein). Our calculations show that

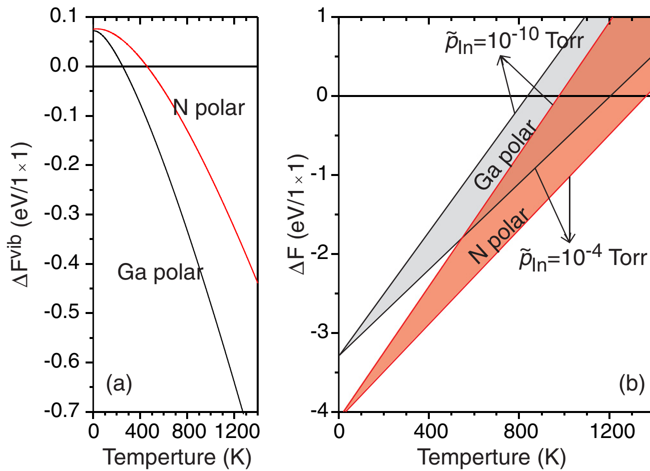

FIG. 5. (Color online) (a) Vibrational entropic contributions to the free energy ΔF^{vib} and (b) free-energy differences ΔF between 2×2 In adl $+$ $\mathrm{In_{Ga}}$ and clean surfaces [as defined by Eq. (9) and in the main text] for In partial pressures $\widetilde{p}_{\mathrm{In}}$ in the range 10^{-10}–10^{-4} Torr as a function of temperature for both Ga- and N-polar surfaces. In (b), the ratio of In and Ga partial pressures $\widetilde{p}_{\mathrm{In}}/\widetilde{p}_{\mathrm{Ga}}$ is 100.

three GaN surface layers are sufficient to determine ΔF^{vib} to within an accuracy better than 1 meV per 1×1 surface unit cell at $T = 1000$ K.

The vibrational contributions to the free energy (ΔF^{vib}) as well as the full surface free energy (ΔF) of the 2×2 In adlayer with $\mathrm{In_{Ga}}$ taken with respect to the clean surface for both (0001) and (000$\bar{1}$) surfaces as a function of temperature are shown in Fig. 5(a). One sees clearly that entropic contributions substantially reduce the surface energy. However, due to stiffer In-N bonds at the N-polar surfaces in comparison to the more metallic and thus softer In-Ga bonds at the Ga-polar surface, ΔF^{vib} at $T = 1000$ K is ≈ 0.26 eV per 1×1 smaller for the Ga-polar surfaces. In Fig. 5(b), the surface free energies of the Ga-polar and N-polar 2×2 In adl $+$ $\mathrm{In_{Ga}}$ surfaces with respect to the corresponding clean surfaces are plotted against temperature for In partial pressures $\widetilde{p}_{\mathrm{In}}$ in the range 10^{-4}–10^{-10} Torr. The ratio of In to Ga partial pressures $\widetilde{p}_{\mathrm{In}}/\widetilde{p}_{\mathrm{Ga}}$ is fixed to 100. Reducing this ratio by two orders of magnitude shifts the equilibrium temperature of the clean and In covered surfaces by less than 40 K. As can be clearly seen, the equilibrium temperature, i.e., the temperature at which the clean and the In covered surfaces are energetically degenerate, is $\approx$ 150 K higher for the N-polar than the Ga-polar surfaces for the same value of $\widetilde{p}_{\mathrm{In}}$. Thus, the N-polar 2×2 In adlayer with $\mathrm{In_{Ga}}$ surface is thermodynamically stable to $\approx$ 150 K higher temperatures than the Ga-polar counterpart. This can be explained in terms of an interplay between the softer but weaker In-Ga bonds at the Ga-polar surface versus the stiffer but stronger In-N bonds at the N-polar surface: The large reduction in the Ga-polar surface free energy caused by the softer In-Ga bonds (≈ 0.26 eV per 1×1) is more than compensated for by the stronger binding of the In adlayer to the N-polar surface (≈ 1.02 eV per 1×1). Hence, chemical effects due to the formation of strong and stiff In-N bonds at N-polar surfaces as compared to weak In-Ga bonds at Ga-polar surfaces are responsible for the higher thermal stability and thus incorporation of In on N-polar surfaces.

V. INDIUM SURFACE SEGREGATION

The enhanced thermodynamic stability of $\mathrm{In_{Ga}}$ in the top surface layer ($\mathrm{L_1}$) for Ga-polar surfaces is a direct indicator of a strong energetic driving force for In segregation to the Ga-polar surface. In the following, we will investigate this by comparing the energetics of a single $\mathrm{In_{Ga}}$ in the top four layers ($\mathrm{L_1}$–$\mathrm{L_4}$) of both Ga- and N-polar surfaces. The difference in energy between an $\mathrm{In_{Ga}}$ in L_i and an $\mathrm{In_{Ga}}$ in $\mathrm{L_4}$ (approximately bulk) is calculated for both polarities and for various In surface coverages:

$$\Delta E^{\mathrm{tot}}_{\mathrm{surf,In_{Ga}:L_4\to L}_i} = E^{\mathrm{tot}}_{\mathrm{surf,L}_i\,\mathrm{In_{Ga}}} - E^{\mathrm{tot}}_{\mathrm{surf,L_4\,In_{Ga}}}, \qquad (10)$$

where $E^{\mathrm{tot}}_{\mathrm{surf,L}_i\,\mathrm{In_{Ga}}}$ is the energy of a supercell for a particular surface with an $\mathrm{In_{Ga}}$ atom in L_i. The In trilayer, although not found to be thermodynamically stable, is also included to identify trends. The case of pseudomorphic growth on GaN is considered first, followed by the lattice-matched case.

The results, plotted in Fig. 6, clearly indicate a strong energetic preference for $\mathrm{In_{Ga}}$ atoms to occupy the first surface layer $\mathrm{L_1}$ for all Ga-polar surface morphologies. This preference is strongest for the clean surface ($\Delta E \approx 1.5$ eV) and becomes progressively smaller as a function of increasing surface coverage, with the smallest energy gain found for an $\mathrm{In_{Ga}}$ atom occupying $\mathrm{L_1}$ beneath an In trilayer ($\Delta E \approx 0.5$ eV). In contrast, for N-polar surfaces, no preference is found for an $\mathrm{In_{Ga}}$ atom to occupy $\mathrm{L_1}$ (i.e., for In surface segregation), with ΔE found to be independent of the layer of $\mathrm{In_{Ga}}$ for all surface coverages.

These observations can be understood in part by strain-relaxation arguments. For Ga-polar surfaces, $\mathrm{In_{Ga}}$ atoms in $\mathrm{L_1}$ can release strain energy by increasing the In-N bond length. This is achieved by relaxing the In atoms in the top

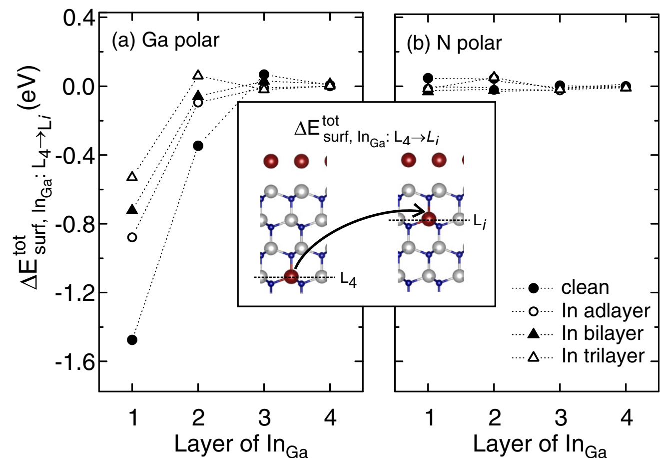

FIG. 6. (Color online) Change in energy as an $\mathrm{In_{Ga}}$ atom is moved from $\mathrm{L_4}$ to $\mathrm{L_1}$, for various surface morphologies (assuming pseudomorphic growth on GaN) for (a) (0001) and (b) (000$\bar{1}$) GaN surfaces. Inset: schematic representation of an $\mathrm{In_{Ga}}$ atom in $\mathrm{L_4}$ (left) and in L_i (right). Small/blue, large/red, and large/gray balls indicate N, In, and Ga atoms, respectively.

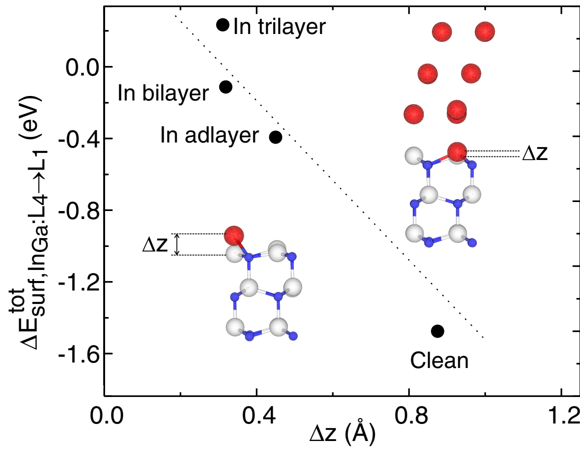

FIG. 7. (Color online) Energy difference $\Delta E^{\text{tot}}_{\text{surf},\text{In}_{\text{Ga}}:\text{L}_4\to\text{L}_1}$ for moving an In_{Ga} atom from layer L_4 to layer L_1 [see Eq. (10)] as a function of the outwards relaxation of In_{Ga} in L_1, Δz [see Eq. (11)], for selected Ga-polar surface morphologies. The dashed line is a guide to the eye.

surface layer outwards, with the relaxation largest for the clean surface. The presence of In adlayer/s, however, which prefer to remain planar to minimize their surface tension, impedes this relaxation, hence the decreasing stability of In_{Ga} atoms in L_1 with increasing In coverage. This effect is elucidated in Fig. 7 where, for the different Ga-polar surface morphologies, $\Delta E^{\text{tot}}_{\text{surf},\text{In}_{\text{Ga}}:\text{L}_4\to\text{L}_1}$ is plotted as a function of the outwards relaxation Δz of the In_{Ga} atom in L_1, where Δz is defined as

$$\Delta z = z_{\text{In}} - z_{\text{Ga}}, \tag{11}$$

where z_{In} is the z coordinate, measured in the [0001] direction, of the In_{Ga} atom and z_{Ga} is the averaged z coordinate of the Ga atoms in L_1. One sees a clear dependence of $\Delta E^{\text{tot}}_{\text{surf},\text{In}_{\text{Ga}}:\text{L}_4\to\text{L}_1}$ on Δz: As the surface coverage is increased from clean to In adlayer, bilayer, and trilayer, Δz is progressively reduced, each time with an associated increase in ΔE.

For the N-polar surface, no outwards relaxation of an In_{Ga} atom in L_1 is found, with the surface N atoms preferring to maintain a flat profile. Our calculations therefore indicate that the energy gain associated with any outwards relaxation of the In_{Ga} atom is in effect fully compensated for by the cost of deforming the surface N layer, and the associated increase in the surface energy. Chemistry also plays a role in explaining the above observations. For N-polar surfaces, In_{Ga} atoms in L_1 experience the same bonding environment as in any other layer, whereas for Ga-polar surfaces, the exchange of an In-N bond for a Ga-N bond stabilizes this configuration. In addition, the stability of an In_{Ga} atom in L_1 will be altered in the presence of an In adlayer where, in comparison to ideal bulk, it gains one additional In-In bond, and loses an In-Ga bond.

To investigate the relative importance of chemistry versus strain for the stability of an In_{Ga} atom in L_1 beneath clean and In adlayer covered Ga-polar and N-polar surfaces, a mechanical/chemical decomposition of $\Delta E^{\text{tot}}_{\text{surf},\text{In}_{\text{Ga}}:\text{L}_4\to\text{L}_i}$ is

TABLE II. Decomposition of $\Delta E^{\text{tot}}_{\text{surf},\text{In}_{\text{Ga}}:\text{L}_4\to\text{L}_i}$ (subscript omitted below for clarity) into mechanical and chemical contributions for a range of surface morphologies. Pseudomorphic growth on GaN is considered.

Ga-polar	L_i	ΔE^{tot}	ΔE^{mech}	ΔE^{chem}
Clean	L_1	−1.48	−0.44	−1.04
	L_2	−0.35	0.08	−0.43
	L_3	0.06	0.20	−0.14
In adlayer	L_1	−0.88	−0.09	−0.79
	L_2	−0.09	0.04	−0.13
	L_3	−0.01	−0.02	0.01
N-polar				
Clean	L_1	0.05	0.17	−0.12
	L_2	0.05	0.04	0.01
	L_3	0.00	−0.01	0.01
In adlayer	L_1	−0.01	0.01	−0.02
	L_2	−0.02	0.02	−0.04
	L_3	−0.02	−0.01	−0.01

performed:

$$\Delta E^{\text{tot}}_{\text{surf},\text{In}_{\text{Ga}}:\text{L}_4\to\text{L}_i} = \Delta E^{\text{mech}}_{\text{surf},\text{In}_{\text{Ga}}:\text{L}_4\to\text{L}_i} + \Delta E^{\text{chem}}_{\text{surf},\text{In}_{\text{Ga}}:\text{L}_4\to\text{L}_i}, \tag{12}$$

$$\begin{aligned}\Delta E^{\text{mech}}_{\text{surf},\text{In}_{\text{Ga}}:\text{L}_4\to\text{L}_i} &= E^{\text{tot}'}_{\text{surf},\text{In}_{\text{Ga}}\,\text{L}_i} - E^{\text{tot}'}_{\text{surf},\text{In}_{\text{Ga}}\,\text{L}_4},\\ \Delta E^{\text{chem}}_{\text{In}_{\text{Ga}}:\text{L}_4\to\text{L}_i} &= \left(E^{\text{tot}}_{\text{surf},\text{In}_{\text{Ga}}\,\text{L}_i} - E^{\text{tot}'}_{\text{surf},\text{In}_{\text{Ga}}\,\text{L}_i}\right)\\ &\quad - \left(E^{\text{tot}}_{\text{surf},\text{In}_{\text{Ga}}\,\text{L}_4} - E^{\text{tot}'}_{\text{surf},\text{In}_{\text{Ga}}\,\text{L}_4}\right),\end{aligned} \tag{13}$$

where $E^{\text{tot}'}_{\text{surf},\text{In}_{\text{Ga}}\,\text{L}_i}$ is the energy of a supercell with atomic coordinates fixed to those of the relaxed In_{Ga} supercell, but with the In_{Ga} atom replaced by a Ga atom [67]. $\Delta E^{\text{mech}}_{\text{In}_{\text{Ga}}:\text{L}_4\to\text{L}_i}$ and $\Delta E^{\text{chem}}_{\text{In}_{\text{Ga}}:\text{L}_4\to\text{L}_i}$ are the mechanical and chemical energies (taken with respect to their values in L_4) associated with exchanging a Ga atom with an In_{Ga} atom. The former represents the change in energy associated with the distortion of the surrounding GaN matrix due to the strain field imposed by the In atom. The latter represents the change in energy associated with changes in bonding due to the In_{Ga} atom, but without the effects of atomic relaxation.

Results are presented in Table II for the case of pseudomorphic growth on GaN. For the Ga-polar clean surface, one sees that both mechanical and chemical contributions are non-negligible for an In_{Ga} atom in L_1, so that both strain relaxation and bonding are responsible for the stability of In_{Ga} in this case. In the presence of an In adlayer (which is the thermodynamically stable surface within the $\text{In}_{0.25}\text{Ga}_{0.75}\text{N}$ growth window), the mechanical and chemical contributions both increase, indicating that both a reduction in strain relaxation and also a less favorable bonding configuration are responsible for the reduced stability in this case. The increase in the mechanical contribution brings this value close to zero, so that the chemical effect now represents the major part of the energetic driving force for surface segregation.

The reduction in $\Delta E^{\text{chem}}_{\text{In}_{\text{Ga}}:\text{L}_4\to\text{L}_1}$ for the case of the In adlayer as compared to the clean surface implies that the In-In bond

formed between an In_{Ga} atom in L_1 and an In atom from the In adlayer is weaker than a Ga-In bond between the same two layers. From the chemical contributions, this additional stability is estimated to be ~0.2 eV. A separate estimate can be made by considering ideal bulk structures that consist of only Ga-In or In-In next-nearest neighbors (with zinc-blende rather than wurzite used to better approximate the strongly directional bonding between an In atom in the adlayer and the Ga or In atom directly below it). From these (fully relaxed) calculations, we also find the In-Ga bond to to be stronger than the In-In bond, with an additional stability of ~0.1 eV.

For the N-polar surface, and within the estimated calculational error of our calculations, $\Delta E^{mech}_{In_{Ga}:L_4\rightarrow L_i}$ and $\Delta E^{chem}_{In_{Ga}:L_4\rightarrow L_i}$ are found to be zero for all layers and for both clean and In adlayer surfaces. The only exception is for the clean surface with an In_{Ga} atom in L_1, for which the mechanical and chemical parts are 0.17 and −0.12 eV, respectively. Apart from this, the ratio of mechanical and chemical contributions is constant for In_{Ga} atoms across all layers and for all N-polar surfaces, consistent with the equivalent bonding environments and degrees of strain relaxation in all cases. For the clean L_1 configuration, a slight increase in In-N bond lengths is in fact found, at the cost of also increasing the Ga-N bond lengths slightly. The deviation from zero of the mechanical and chemical parts in this case implies an incomplete separation of strain relaxation and rebonding contributions between the mechanical and chemical parts. This is an intrinsic problem with any mechanical/chemical decomposition, given that strain relaxation and rebonding effects are intrinsically coupled. The estimated error of $\pm \sim 0.1$ eV is, however, sufficiently small to not alter our conclusions.

For the second considered scenario, lattice-matched $In_{0.25}Ga_{0.75}N$, the energetics of subsurface In_{Ga} as a function of surface polarity and morphology are qualitatively identical to the pseudomorphic to GaN case. The effect is reduced slightly for the Ga-polar surface, however, with the stability of the In_{Ga} atom in L_1 as compared to L_4 being in general smaller than for the pseudomorphic to GaN case. The reduction in stability is ~0.2 eV for the clean and In adlayer surfaces, approximately 0.1 eV for the In bilayer surface, but zero for the case of the In trilayer. This reduced stability is consistent with the larger in-plane lattice parameters of the lattice-matched case, so that there is less strain energy for a bulk In_{Ga} atom to release by moving to L_1. The increased energy difference for the pseudomorphic to GaN Ga-polar surface compared to the lattice-matched Ga-polar surface implies that In segregation will be a function of surface strain modulations. As a consequence, enhanced In segregation is expected in regions of compressive strain.

In our discussions so far, the enhanced stability of In_{Ga} in L_1 for Ga-polar surfaces has been taken to imply enhanced In surface segregation for Ga-polar surfaces. Such segregation could occur as a III-N layer containing an In_{Ga} atom is covered by a new III-N layer during step-flow growth, with the In_{Ga} atom exchanging positions with a Ga atom from the new layer during this process. However, if a fast enough growth rate was used, then such a transition will be kinetically suppressed, so that In surface segregation might be significantly reduced.

VI. CONCLUSIONS

In extending the well-established concepts of *ab initio* derived surface phase diagrams from chemically ordered binaries to disordered ternary alloys, we came across several phenomena that appear to be specific for alloys consisting of constituents that are poorly matched both with respect to chemistry and atomic size. For the case of coherent epitaxially grown InGaN alloy films as considered here, these findings have severe consequences and shed some light on the challenges commonly observed when growing them. First, the thermodynamically allowed range of chemical potentials for pseudomorphic $In_{0.25}Ga_{0.75}N$ grown on GaN is found to be two orders of magnitude smaller than the corresponding range for GaN growth. Second, our calculations show that the significantly reduced growth window can be widened by growing not on pure GaN but on InGaN alloys. For the case considered here, namely, $In_{0.25}Ga_{0.75}N$ growth on lattice-matched heterointerfaces (with in-plane lattice parameters of $In_{0.25}Ga_{0.75}N$), the growth window is widened by a factor of 3 in each of the chemical potentials, and is shifted towards moderate In-rich/moderate Ga-poor growth conditions.

For both surface polarities, fully incorporated $In_{0.25}Ga_{0.75}N$ underneath an In adlayer is found to be thermodynamically stable within the $In_{0.25}Ga_{0.75}N$ growth window. However, the stronger binding of the In adlayer to the N-polar surface extends the thermal stability of the incorporated In to $\approx$ 150 K higher temperatures than for the Ga-polar surface. Furthermore, for Ga-polar growth, additional In_{Ga} atoms are stabilized in the first III-N layer, in contrast to N-polar growth where a stoichiometric In/Ga ratio is found in all layers. The latter implies enhanced In surface segregation for Ga-polar growth, which combined with the reduced thermal stability of incorporated In for this polarity is detrimental to the growth of InGaN-films with high In content. In contrast, growing InGaN on N-polar surfaces should allow one to use higher growth temperatures due to the enhanced thermodynamic stability of incorporated In. The higher growth temperature is beneficial for surface kinetics and will result in higher crystal quality as well as higher In concentrations due to the higher solubility of In. These conclusions are in good accord with experimental findings [15–18].

The driving force for In surface segregation for Ga-polar growth was investigated in terms of a mechanical/chemical decomposition of the energy, and was found to originate in part from a release of strain energy, due to the sizable misfit between In and Ga atoms, but mainly due to a more favorable bonding configuration, due to stronger Ga-N bonds as compared to In-N bonds. In addition, the effect was found to be stronger for the case of pseudomorphic growth on GaN than for the lattice-matched case, on account of the more efficient strain accommodation of In_{Ga} in the latter case. This dependance of the energetic driving force for In segregation on the in-plane strain implies enhanced In segregation in regions of compressive strain. The latter is consistent with previous growth experiments which provided strong evidence of enhanced In incorporation upon relaxation of compressive strain [67].

The driving force for In surface segregation to the Ga-polar surface will only result in actual surface segregation if the

necessary interchange of In and Ga atoms is able to occur, i.e., that the process in which an In atom is brought to the first III-N layer and/or to an on-top position is not kinetically prohibited. Such an exchange is most likely to occur for In atoms in the first III-N layer, either by diffusing upwards to an on-top position or during step-flow growth by exchange of the In atom with a Ga atom at the step edge. In both cases, a strategy for reducing the probability of such an exchange occurring would be to increase the step-edge growth rate. However, increased growth rates increase the surface roughness and result in poor surface morphologies. An alternative route might be to achieve lattice-matched growth so that excess In content can be more efficiently kinetically stabilized.

ACKNOWLEDGMENTS

A.D. acknowledges financial support from the EU Marie Curie Industry-Academia Partnerships and Pathways project SINOPLE. L.L. acknowledges financial support from from the European Union Seventh Framework Programme ALIGHT under Grant Agreement No. 280587.

[1] J. Wu, W. Walukiewicz, K. M. Yu, J. W. Ager, E. E. Haller, H. Lu, W. J. Schaff, Y. Saito, and Y. Nanishi, Appl. Phys. Lett. **80**, 3967 (2002).
[2] T. Matsuoka, H. Okamoto, M. Nakao, H. Harima, and E. Kurimoto, Appl. Phys. Lett. **81**, 1246 (2002).
[3] P. Rinke, M. Scheffler, A. Qteish, M. Winkelnkemper, D. Bimberg, and J. Neugebauer, Appl. Phys. Lett. **89**, 161919 (2006).
[4] B. Monemar, J. P. Bergman, I. A. Buyanova, W. Li, H. Amano, and I. Akasaki, MRS Internet J. Nitride Semicond. Res. **1**, U15 (1996).
[5] F. A. Ponce and D. P. Bour, Nature (London) **386**, 351 (1997).
[6] S. Nakamura, M. Senoh, S. Nagahama, N. Iwasa, T. Yamada, T. Matsushita, H. Kiyoku, and Y. Sugimoto, Jpn. J. Appl. Phys. **35**, L74 (1996).
[7] C. J. Neufeld, N. G. Toledo, S. C. Cruz, M. Iza, S. P. DenBaars, and U. K. Mishra, Appl. Phys. Lett. **93**, 143502 (2008).
[8] O. Jani, I. Ferguson, C. Honsberg, and S. Kurtz, Appl. Phys. Lett. **91**, 132117 (2007).
[9] J. Wu, W. Walukiewicz, K. M. Yu, W. Shan, J. W. Ager, E. E. Haller, H. Lu, W. J. Schaff, W. K. Metzger, and S. Kurtz, J. Appl. Phys. **94**, 6477 (2003).
[10] G. B. Stringfellow, J. Cryst. Growth **312**, 735 (2010).
[11] C. S. Gallinat, G. Koblmüller, J. S. Brown, and J. S. Speck, J. Appl. Phys. **102**, 064907 (2007).
[12] J. Lang and J. Speck, J. Cryst. Growth **346**, 50 (2012).
[13] M. Siekacz, M. Sawicka, H. Turski, G. Cywinski, A. Khachapuridze, P. Perlin, T. Suski, M. Bockowski, J. Smalc-Koziorowska, M. Krysko, R. Kudrawiec, M. Syperek, J. Misiewicz, Z. Wasilewski, S. Porowski, and C. Skierbiszewski, J. Appl. Phys. **110**, 063110 (2011).
[14] H. Morkoç, *Handbook of Nitride Semiconductors and Devices*, Vol. 1 (Wiley, Weinheim, 2009).
[15] S. Keller, N. A. Fichtenbaum, M. Furukawa, J. S. Speck, S. P. Denbaars, and U. K. Mishra, Appl. Phys. Lett **90**, 191908 (2007).
[16] D. N. Nath, E. Guer, S. A. Ringel, and S. Rajan, J. Vac. Sci. Technol. B **29**, 021206 (2011).
[17] D. N. Nath, E. Guer, S. A. Ringel, and S. Rajan, Appl. Phys. Lett **97**, 071903 (2010).
[18] K. Xu and A. Yoshikawa, Appl. Phys. Lett. **83**, 251 (2003).
[19] G. Koblmüller, C. S. Gallinat, S. Bernardis, J. S. Speck, G. D. Chern, E. D. Readinger, H. Shen, and M. Wraback, Appl. Phys. Lett. **89**, 071902 (2006).
[20] G. Koblmüller, C. S. Gallinat, and J. S. Speck, J. Appl. Phys. **101**, 083516 (2007).
[21] H. Naoi, F. Matsuda, T. Araki, A. Suzuki, and Y. Nanishi, J. Cryst. Growth **269** 155 (2004).
[22] D. Segev and C. G. V. de Walle, Surf. Sci. **601**, L15 (2007).
[23] T. Ito, T. Akiyama, and K. Nakamura, J. Cryst. Growth **311**, 3093 (2009).
[24] V. Timon, S. Brand, S. J. Clark, and R. A. Abram, J. Phys.: Condens. Matter **17**, 17 (2005).
[25] V. Timon, S. Brand, S. J. Clark, and R. A. Abram, J. Phys.: Condens. Matter **16**, 531 (2004).
[26] A. Ishii, Appl. Surf. Sci. **216**, 447 (2003).
[27] K. Rapcewicz, M. Buongiorno Nardelli, and J. Bernholc, Phys. Rev. B **56**, R12725 (1997).
[28] J. E. Northrup, J. Neugebauer, R. M. Feenstra, and A. R. Smith, Phys. Rev. B **61**, 9932 (2000).
[29] F.-H. Wang, P. Krüger, and J. Pollmann, Phys. Rev. B **64**, 035305 (2001).
[30] A. L. Rosa and J. Neugebauer, Phys. Rev. B **73**, 205346 (2006).
[31] A. R. Smith, R. M. Feenstra, D. W. Greve, J. Neugebauer, and J. E. Northrup, Phys. Rev. Lett. **79**, 3934 (1997).
[32] Q.-K. Xue, Q. Z. Xue, R. Z. Bakhtizin, Y. Hasegawa, I. S. T. Tsong, T. Sakurai, and T. Ohno, Phys. Rev. Lett. **82**, 3074 (1999).
[33] C. G. Van de Walle and J. Neugebauer, Phys. Rev. Lett. **88**, 066103 (2002).
[34] A. R. Smith, R. M. Feenstra, D. W. Greve, M. S. Shin, M. Skowronski, J. Neugebauer, and J. E. Northrup, Surf. Sci. **423**, 70 (1999).
[35] C. K. Gan and D. J. Srolovitz, Phys. Rev. B **74**, 115319 (2006).
[36] J. E. Northrup and C. G. V. de Walle, Appl. Phys. Lett. **84**, 4322 (2004).
[37] J. Neugebauer, T. K. Zywietz, M. Scheffler, J. E. Northrup, H. Chen, and R. M. Feenstra, Phys. Rev. Lett. **90**, 056101 (2003).
[38] H. Chen, R. M. Feenstra, J. E. Northrup, T. Zywietz, J. Neugebauer, and D. W. Greve, J. Vac. Sci. Technol. B **18**, 2284 (2000).
[39] C. K. Gan and D. J. Srolovitz, Phys. Rev. B **77**, 205324 (2008).
[40] J. E. Northrup and J. Neugebauer, Phys. Rev. B **60**, R8473 (1999).
[41] J. E. Northrup, Phys. Rev. B. **79**, 041306 (2009).
[42] J. E. Northrup, Appl. Phys. Lett. **95**, 133107 (2009).
[43] Ž. Gačević, V. J. Gómez, N. García Lepetit, P. E. D. Soto Rodríguez, A. Bengoechea, S. Fernández-Garrido, R. Nötzel, and E. Calleja, J. Cryst. Growth **364**, 123 (2013).

[44] M. Siekacz, M. L. Sza'nkowska, A. Feduniewicz-Zmuda, J. Smalc-Koziorowska, G. Cywi'nski, S. Grzanka, Z. R. Wasilewski, I. Grzegory, B. Lucznki, S. Porowski, and C. Skierbiszewsk, Phys. Status Solidi **6**, S917 (2009).
[45] M. Siekacz, A. Feduniewicz-Zmuda, G. Cywi'nski, M. Kry'sko, I. Grzegory, S. Krukowski, K. E. Waldrip, W. Jantsch, Z. R. Wasilewski, S. Porowski, and C. Skierbiszewski, J. Cryst. Growth **310**, 3983 (2008).
[46] C. Skierbiszewski, Z. R. Wasilewski, I. Grzegory, and S. Porowski, J. Cryst. Growth **311**, 1632 (2009).
[47] A concentration of 25% In can be well represented by a 2×2 surface unit cell (which emerges as the most favorable choice of in-plane dimensions within the $In_{0.25}Ga_{0.75}N$ growth window). Specifically, In_{Ga} atoms can be arranged, one per 2×2 surface unit cell, per layer, in a semirandom manner. A good representation of bulk In_{Ga} is important as it enables proper consideration of competing concentrations and configurations of In_{Ga} (e.g., in the first III-N layers), and achieving such a distribution for high In concentrations and for computationally amenable supercell sizes was not possible for other choices of In concentrations.
[48] A. Kobayashi, J. Ohta, and H. Fujioka, J. Appl. Phys. **99**, 123513 (2006).
[49] N. Li, W. S.-J, E.-H. Park, Z. C. Feng, H.-L. Tsai, Y. J.-R, and I. Ferguson, J. Cryst. Growth **311**, 4628 (2009).
[50] P. Hohenberg and W. Kohn, Phys. Rev. **136**, B864 (1964).
[51] W. Kohn and L. J. Sham, Phys. Rev. **140**, A1133 (1965).
[52] P. E. Blöchl, Phys. Rev. B **50**, 17953 (1994).
[53] G. Kresse and D. Joubert, Phys. Rev. B **59**, 1758 (1999).
[54] H. Monkhorst and J. Pack, Phys. Rev. B **13**, 5188 (1976).
[55] C. K. Gan, Y. P. Feng, and D. J. Srolovitz, Phys. Rev. B **73**, 235214 (2006).
[56] A. Zoroddu, F. Bernardini, P. Ruggerone, and V. Fiorentini, Phys. Rev. B **64**, 045208 (2001).
[57] A. Tabata, L. K. Teles, L. M. R. Scolfaro, J. R. Leite, A. Kharchenko, T. Frey, D. J. As, D. Schikora, K. Lischka, J. Furthmüller, and F. Bechstedt, Appl. Phys. Lett. **80**, 769 (2002).
[58] A. Fischer, H. Kühne, and H. Richter, Phys. Rev. Lett. **73**, 2712 (1994).
[59] T. J. Anderson and I. Ansara, J. Phase Equilib. **12**, 64 (1991).
[60] D. Segev and C. G. V. de Walle, J. Cryst. Growth **300**, 199 (2007).
[61] R. González-Hernández, W. López-Pérez, M. G. Moreno-Armenta, and Jairo Arbey Rodríguez M., Phys. Rev. B **81**, 195407 (2010).
[62] G. B. Stringfellow, J. Cryst. Growth **115**, 1 (1991).
[63] R. Heckingbottom, C. J. Todd, and G. J. Davies, J. Electrochem. Soc. **127**, 444 (1980).
[64] M. V. Durnev, A. V. Omelchenko, E. V. Yakovlev, I. Yu. Evstratov, and S. Yu. Karpov, Appl. Phys. Lett. **97**, 051904 (2010).
[65] D. C. Wallace, *Thermodynamics of Crystals* (Dover, New York, 1998).
[66] B. Grabowski, T. Hickel, and J. Neugebauer, Phys. Rev. B **76**, 024309 (2007).
[67] The mechanical and chemical contributions presented here are not absolute but are instead taken with respect to their values corresponding to an In_{Ga} atom in L_4 (the fourth III-N layer). $\Delta E^{tot}_{surf,In_{Ga}:L_4 \to L_i}$ is the total energy difference between an In_{Ga} atom in L_1 and L_4, so that the corresponding mechanical energy can be written $\Delta E^{mech}_{surf,In_{Ga}:L_4 \to L_i} = (E^{tot'}_{surf,In_{Ga}\,L_i} - E^{tot}_{surf}) - (E^{tot'}_{surf,In_{Ga}\,L_4} - E^{tot}_{surf})$, with the second and fourth terms canceling out to give the mechanical part as presented in Eq. (13). The chemical energy can then be written $\Delta E^{chem}_{surf,In_{Ga}:L_4 \to L_i} = \Delta E^{tot}_{surf,In_{Ga}:L_4 \to L_i} - \Delta E^{mech}_{surf,In_{Ga}:L_4 \to L_i} = (E^{tot}_{surf,In_{Ga}\,L_i} - E^{tot}_{surf,In_{Ga}\,L_4}) - (E^{tot'}_{surf,In_{Ga}\,L_i} - E^{tot'}_{surf,In_{Ga}\,L_4})$, also consistent with Eq. (13).